
Adaptive Image Quality Assessment via Teaching Large Multimodal Model to Compare

Hanwei Zhu^{*†1} Haoning Wu^{*2} Yixuan Li¹ Zicheng Zhang³ Baoliang Chen¹
 Lingyu Zhu¹ Yuming Fang⁴ Guangtao Zhai³ Weisi Lin² Shiqi Wang^{1‡}

¹ City University of Hong Kong

² Nanyang Technological University

³ Shanghai Jiao Tong University

⁴ Jiangxi University of Finance and Economics

<https://compare2score.github.io/>

Abstract

While recent advancements in large multimodal models (LMMs) have significantly improved their abilities in image quality assessment (IQA) relying on *absolute* quality rating, how to transfer reliable *relative* quality comparison outputs to continuous perceptual quality scores remains largely unexplored. To address this gap, we introduce **Compare2Score**—an all-around LMM-based no-reference IQA (NR-IQA) model, which is capable of producing qualitatively comparative responses and effectively translating these discrete comparative levels into a continuous quality score. Specifically, *during training*, we present to generate scaled-up comparative instructions by comparing images from the same IQA dataset, allowing for more flexible integration of diverse IQA datasets. Utilizing the established large-scale training corpus, we develop a human-like visual quality comparator. *During inference*, moving beyond binary choices, we propose a soft comparison method that calculates the likelihood of the test image being preferred over multiple predefined anchor images. The quality score is further optimized by maximum a posteriori estimation with the resulting probability matrix. Extensive experiments on nine IQA datasets validate that the **Compare2Score** effectively bridges **text-defined comparative levels** during training with converted **single image quality score** for inference, surpassing state-of-the-art IQA models across diverse scenarios. Moreover, we verify that the probability-matrix-based inference conversion not only improves the rating accuracy of **Compare2Score** but also zero-shot general-purpose LMMs, suggesting its intrinsic effectiveness.

1 Introduction

Image quality assessment (IQA) models aim to establish a quantitative mapping between digital visual images and human subjective evaluations, playing an indispensable role across various image processing and computer vision tasks [1]. No-reference IQA (NR-IQA) [2, 3, 4, 5], which evaluate images without a reference, are particularly valuable for real-world applications. Recently, NR-IQA has experienced profound improvement through advanced deep neural networks (DNNs) [6, 7, 8, 9, 10]. However, a primary challenge with current models [8, 11, 12] lies in their limited *cross-distortion* generalization capability since the training and testing data contain significant distribution shift.

*Equal contribution

†Work done during the visit to NTU

‡Corresponding author: shiqiwan@cityu.edu.hk

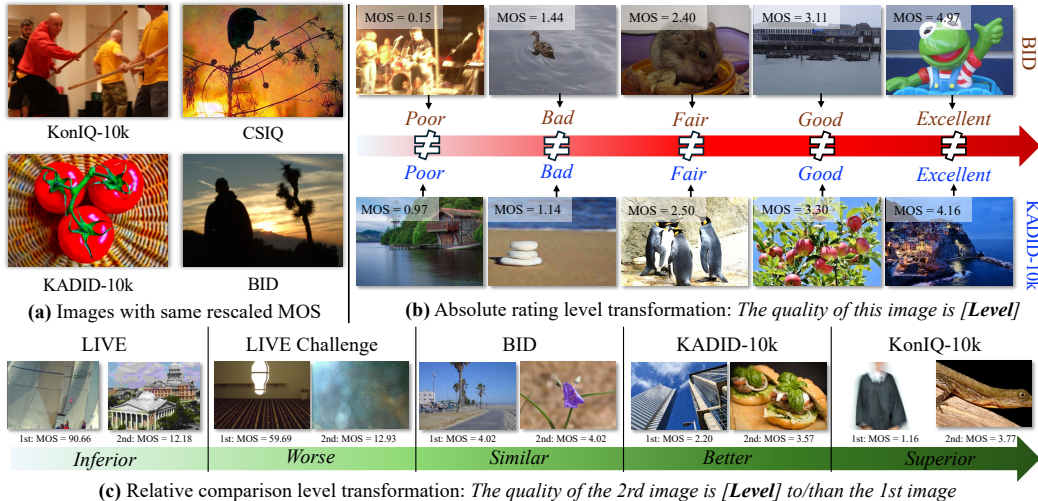


Figure 1: Illustrations of the motivation of this work. (a) Images with identical rescaled MOS from various IQA datasets exhibit significant variations in perceptual quality. (b) Images that cluster at the same rating level from different IQA datasets display mismatches due to differing subjective testing methodologies. (c) By comparing MOSs within the same dataset, it facilitates the flexible combination of multiple IQA datasets.

To improve the generalization capability of the NR-IQA, lots of advanced training techniques have been adopted, such as meta learning [13], domain adaptation [14], test-time adaption [15], and hard example mining [16]. More capable foundation models, such as CLIP [10] and large multimodal models (LMMs) [12], are also proven to be effective in improving generalization ability. Despite these advancements, the gains from such techniques remain constrained due to the persistent **data challenge** inherent in IQA. Alternatively, expanding the IQA training datasets—both in terms of the number of images and the diversity of distortions—emerges as a scalable strategy to augment model robustness [17]. This data scaling law has also been recognized as one of the key factors in building effective LMMs [18, 19, 20, 21, 22, 23]. As such, addressing how to effectively combine existing IQA datasets to meet the extensive data requirements of training LMMs is highly desirable.

As an early attempt of LMMs on IQA, Q-Align [12] proposed to combine different IQA datasets with *absolute* quality ratings. While absolute ratings are widely used for collecting human opinions on different IQA datasets, it is non-trivial to directly fuse them for LMM training. This difficulty arises because each dataset has **different perceptual scales** owing to varying subjective testing methodologies. As shown in Fig. 1 (a), images with identical mean opinion score (MOS) (2.3, all rescaled to range [0, 5]) from four datasets [24, 25, 26, 7] differ significantly in perceptual quality. As a result, despite clustering at the same rating level, these images from different datasets display distinctly different visual qualities (see Fig. 1 (b)). Therefore, simply scaling up the training data by mixing existing IQA datasets with rescaled MOS is fundamentally flawed. Instead, the *relative* quality ranking (*e.g.*, paired comparison) offers intrinsic simplicity and reliability over absolute quality rating [27]. As shown in Fig. 1 (c), it is comparable to the images from the same IQA datasets as their MOSs originate from the same subjective user study, facilitating a more flexible combination of various IQA datasets. However, the key limitation of the paired comparison method is its impracticality in deriving individual image quality scores from $\binom{M}{2}$ comparisons when M is large. Furthermore, the lack of effective and efficient methods to convert *relative* comparisons into quantitative *absolute* ratings makes current comparison-based approaches difficult to apply to real-world scenarios.

To tackle these challenges, this paper leverages the flexibility and reliability of relative quality comparisons to introduce **Compare2Score**—an all-around LMM-based NR-IQA model, which is designed to generate human-like qualitative comparisons and compute effective quality scores. Before delving into detail, we clearly highlight our main contributions as follows.

- **[A repurposed training dataset.]** We present to generate scaled-up comparative instructions by comparing MOSs of images within each IQA dataset, which allows for more flexible

integration of diverse IQA datasets. Specifically, the approach simulates subjective testing by posing the question, “Compared with the first image, how is the quality of the second image?” (see Fig. 1 (c)). Responses are then generated based on the MOS comparisons of the image pairs. Using the empirical rule, we categorize the image pairs into five distinct comparative levels: inferior, worse, similar, better, superior. This method produces a comprehensive training dataset that enables the LMM to effectively handle various distortion scenarios, resulting in a human-like **visual quality comparator**.

- **[An inference conversion strategy.]** We develop an **adaptive soft comparison scheme** that efficiently translates discrete comparative levels into continuous quality scores. Unlike traditional two-alternative forced choice (2AFC) methods, our approach calculates the likelihood that an input image is preferred over multiple anchor images. This probability is derived from a weighted summation of the softmax-transformed log probabilities across five comparative levels. Subsequently, the quality score of the input image is calculated through maximum a posteriori (MAP) estimation based on the resulting probability matrix.
- **[A state-of-the-art framework.]** We conduct extensive experiments to validate the effectiveness of teaching the relative quality ranking knowledge to LMM. The proposed model, namely **Compare2Score**, consistently outperforms state-of-the-art NR-IQA models on both synthetic and realistic distortions and shows enhanced generalization capability across different cross-distortion scenarios. Furthermore, we demonstrate that the probability matrix-based inference conversion significantly enhances the rating accuracy of **Compare2Score** and extends these improvements to zero-shot general-purpose LMMs.

2 Related Work

2.1 NR-IQA Models

Regressing for NR-IQA Traditional learning-to-regress NR-IQA models [28, 29, 30, 31] build effective quality-aware feature extractors rooted in theoretical principles, which are then mapped to quality scores through well-trained IQA regressors. In contrast, deep-learning-based IQA models [6, 9, 32, 33] exploit large volumes of IQA data to simultaneously refine DNNs for both feature extraction and quality regression. By using advanced training techniques, such as domain adaption [5], meta-learning [13], multi-task learning [34, 10], and contrastive learning [32], NR-IQA models show high correlation with the HVS. However, these models show limited cross-distortion ability. Additionally, these models typically produce quantitative quality scores, creating a significant gap from subjective user studies that prefer learning and assigning text-defined quality levels [35].

Ranking for NR-IQA Beyond learning-to-regress schemes, many models address IQA through a relative quality ranking setting [36, 37, 38, 17, 10]. Liu *et al.* [37] synthesized a large IQA dataset labeled with distortion types and levels to train a Siamese network for precise image quality ranking. Zhang *et al.* [17] incorporated probabilistic quality preference for image pairs from diverse datasets to address inter-dataset incomparable concerns. LIQE utilized a pairwise learning-to-rank training strategy with both visual and textual inputs [10]. Such ranking-based models mitigate the vulnerability towards task-agnostic information of regressing-based models, enabling more robust capabilities for different distortion scenarios [17, 10]. Nevertheless, the application of the learning-to-rank scheme for LMM is largely under-explored. As such, we present to leverage relative comparisons to develop an LMM-based NR-IQA model that produces qualitative comparison outcomes and translates the discreet comparative levels into continuous quality scores effectively.

2.2 LMMs for IQA

Recently, many works have explored the capabilities of LMMs on IQA, covering both benchmarking [39, 40, 41, 42] and refining [39, 12, 43, 44, 45, 46]. Wu *et al.* laid the groundwork by examining and instructing of LMMs in low-level vision tasks, through the development of Q-Bench [47] and Q-Instruct [39], respectively. Wu *et al.* analyzed LMM’s performance under various standardized prompting settings [42], validating the effectiveness of chain-of-thought prompting in IQA tasks. Co-Instruct [46] extended the low-level visual capability of the LMM to meet the requirement of multiple image inputs. Despite demonstrating success, the qualitative outputs of the above LMMs are hard to transfer to a quantitative score, which often plays an important role in computer vision

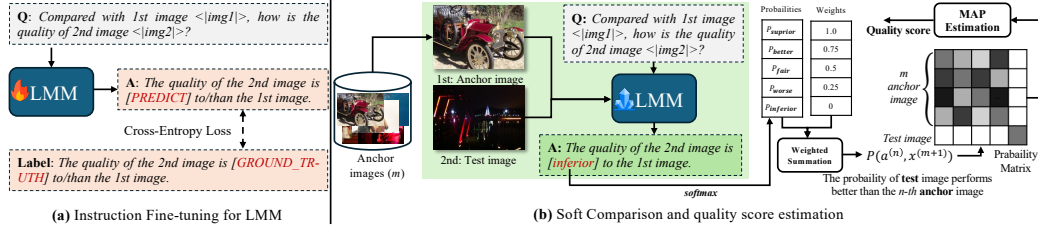


Figure 2: Training and inference phase of **Compare2Score**. (a) The LMM is fine-tuned with instruction-response pairs generated by comparing the MOSs from the same IQA dataset, allowing for a more flexible combination of various IQA datasets. (b) The trained visual quality comparator (*i.e.*, LMM) is utilized to compute the likelihood of a test image being preferred over the anchor images, and then the quality score is derived using MAP estimation.

tasks [48]. Q-Align [12] made the first attempt by transferring the qualitative rating levels to the perceptual quality scores. However, as shown in Figs. 1 (a) & (b), it is impractical to expand the training dataset by simply mixing multiple IQA datasets with rescaled MOS. Therefore, we introduce a novel relative ranking strategy that allows for the seamless integration of existing IQA datasets into an expanded training set, which is then utilized to train an LMM-based visual quality comparator.

3 The Compare2Score Framework

In this section, we first describe the preliminaries of paired comparison for humans and LMMs, respectively. Subsequently, we introduce our methodological framework, which includes generating the training data with quantitatively comparative instructions (Sec. 3.2), the LMM-based visual quality comparator (Sec. 3.3), and the soft comparison method for quality score derivation (Sec. 3.4). Fig. 2 shows the training and testing diagrams of **Compare2Score** framework.

3.1 Preliminaries

Paired Comparison for Humans. The paired comparison methodology in subjective testing involves three principal steps: the combination of images, the collection of human judgments, and the aggregation of these judgments into quality scores. In particular, given a set of images $\mathcal{X} = \{(x^{(i)}, q^{(i)})\}_{i=1}^M$ where $x^{(i)} \in \mathbb{R}^N$ is the image and $q^{(i)} \in \mathbb{R}$ represents the ground-truth quality score, the methodology requires comparing a total of $\binom{M}{2}$ pairs. We assume that a higher $q^{(i)}$ indicates better perceptual quality. The outcomes of these comparisons are recorded in a count matrix $C \in \mathbb{R}^{M \times M}$, where each entry records the number of times one image is preferred over another. The global ranking scores $\hat{q} = \{\hat{q}^{(i)}\}_{i=1}^M$ can be computed by MAP estimation [49]:

$$\arg \max_{\hat{q}} \mathcal{L}(\hat{q}|C) + \log p(\hat{q}), \text{ s.t. } \sum_i \hat{q}^{(i)} = 0, \quad (1)$$

where $\mathcal{L}(\cdot)$ denotes the log-likelihood function and $p(\hat{q})$ is a prior on the scale values. Although effective [27], the key limitation of paired comparison is the exponential growth in the number of comparisons, which becomes labor-intensive and costly for large M . Moreover, once the experiment concludes, incorporating new test images for quality score inference becomes almost infeasible.

Paired Comparison for LMMs. Inspired by the efficacy and reliability of paired comparison experiments with humans, we explore the feasibility of adapting this approach for LMMs. Accordingly, we adopt a similar pipeline to that used in subjective testing. The framework for training LMMs and predicting quality scores also involves three core steps: constructing instruction-response pairs, fine-tuning the LMM with such pairs, and inferring quality scores. To increase the efficiency and feasibility of the model, we propose an adaptive soft comparison approach by computing the probability of the test image $x^{(i)}$ being preferred over m representative anchor images. The probability is calculated by a weighted summation of the softmax of the log probabilities across five comparative levels. The outcome of the LMM is a probability matrix, $P \in \mathbb{R}^{(m+1) \times (m+1)}$ where $m \ll M$. The quality score of the input image is then computed by MAP estimation with the same optimization problem as Eqn. (1).

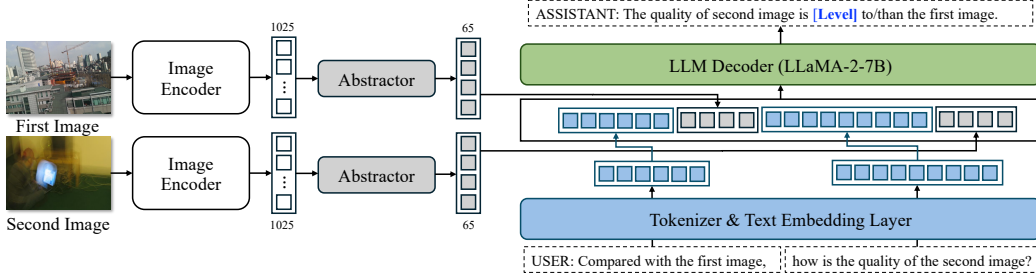


Figure 3: Architecture of the proposed **Compare2Score**. Images are initially processed by an image encoder, followed by token reduction through an abstractor module. The aligned textual and visual embedding are interleaved and processed by the large language model (LLM) decoder to generate precise qualitative comparative levels for paired comparisons.

3.2 Training Dataset: Comparative Instruction-Response Pairs

To facilitate the reasonability of mixing different IQA datasets, we present to compare the visual quality of pairs of images within each IQA dataset. It allows a seamless combination of K established IQA databases for generating large-scale repurposed training dataset (*i.e.*, instruction-response pairs). This process involves translating MOSs into discrete comparative levels. Utilizing the empirical rule [50], we define five levels of comparison: inferior, worse, similar, better, superior. The format of the instruction-response pairs is specified as follows:

USER: Compared with the first image <img1>, how is the quality of the second image <img2>?

ASSISTANT: The quality of the second image is [Level] to/than the first image.

Specifically, we randomly sampling n_k image pairs $\{(x_k^{(i)}, x_k^{(j)})\}_{i,j=1}^{n_k}$ from each database. For each pair $\{(x^{(i)}, x^{(j)})\}$, relative quality rankings are inferred based on MOS and its standard deviation. We assume the perceptual quality of each image $x^{(i)}$ as a Gaussian distribution, characterized by mean $q^{(i)}$ and standard deviation $\sigma^{(i)}$, derived from subjective testing.

Assuming independence in quality variability between images, the quality differential also follows a Gaussian distribution with mean $q^{(ij)} = q^{(i)} - q^{(j)}$ and standard deviation $\sigma^{(ij)} = \sqrt{(\sigma^{(i)})^2 + (\sigma^{(j)})^2}$. This methodology, summarized in Eqn. (2), introduces significance thresholds at $\pm\sigma^{(ij)}$ and $\pm 2\sigma^{(ij)}$, effectively categorizing the quality differences into meaningful comparative levels. These thresholds function similarly to confidence intervals in statistical hypothesis testing, establishing a robust framework for accurately identifying significant perceptual differences between images.

$$\text{Level} = \begin{cases} \text{inferior} & \text{if } q^{(ij)} > 2\sigma^{(ij)}, \\ \text{worse} & \text{if } \sigma^{(ij)} < q^{(ij)} \leq 2\sigma^{(ij)}, \\ \text{similar} & \text{if } -\sigma^{(ij)} < q^{(ij)} \leq \sigma^{(ij)}, \\ \text{better} & \text{if } -2\sigma^{(ij)} < q^{(ij)} \leq -\sigma^{(ij)}, \\ \text{superior} & \text{if } q^{(ij)} < -2\sigma^{(ij)} \end{cases} \quad (2)$$

3.3 Structure: Multi-image LMM as Visual Quality Comparator

The visual quality comparator forms a central element within the **Compare2Score** framework and is tasked with predicting qualitative judgments for pairs of images. As shown in Fig. 3, the architecture incorporates the advanced mPLUG-Owl-2 model [20], which comprises the image encoder (f_ψ), the image abstractor (f_δ), and the large language model (LLM) decoder (g_ϕ). The process begins with the image encoder transforming each image into a visual embedding. This embedding is then dimensionally reduced by the image abstractor to facilitate the handling of multiple images, expressed as $z^{(i)} = f_\delta(f_\psi(x^{(i)}))$, where $z^{(i)} \in \mathbb{R}^U$ with $U = 65$, significantly less than LLaMA-2's maximum context length of 2,048 [51]. These compact visual embeddings are combined with textual embeddings $t \in \mathbb{R}^V$ from the text tokenizer and projected into a shared semantic space. The LLM decoder takes the aligned features and interleaved them to produce the qualitative output, formalized as $\text{Output} = g_\phi(\langle z^{(i)}, t \rangle)$, where $\langle \cdot, \cdot \rangle$ represents the feature alignment.

3.4 Inference Conversion: Adaptive Soft Comparison

Soft Comparison Methodology. After training, the response is determined by selecting the token with the highest probability from the LLM decoder. This conventional method, while straightforward, may not fully exploit the nuanced capabilities of LLMs, as it relies solely on the most probable outcome and disregards other informative probabilities. To overcome this limitation, we propose a soft comparison method that integrates the logits of all five comparative tokens $\mathcal{T} = \{t_i\}_{i=1}^5 = \{\text{inferior, worse, similar, better, superior}\}$. The probability of each token is achieved by the softmax function, expressed as $p_{e^{t_i}} = e^{t_i} / \sum_{j=1}^5 e^{t_j}$, where $p_{e^{t_i}}$ indicate the probability of i -th token. Moreover, to enhance the efficiency and feasibility of the model, we do not compare the test image against every image in the dataset. Instead, we identify a smaller set of anchor images from the training set, denoted as $\mathcal{A} = \{a^{(n)}\}_{n=1}^m$, where $a^{(n)}$ represents the n -th anchor image. As a result, the probability of the test image being preferred over the anchor images is computed by the weighted summation:

$$P_{e^{t_i}}(a^{(n)}, x^{(m+1)}) = \sum_{i=1}^5 w_i p_{e^{t_i}}(a^{(n)}, x^{(m+1)}), \quad n = 1 \dots m, \quad (3)$$

where w_i are predefined weights $\{w_i\}_{i=1}^5 = \{0, 0.25, 0.5, 0.75, 1\}$, facilitating nuanced interpretation and use of the comparative levels.

Anchor Image Selection. We initially partition the IQA dataset into α quality intervals, represented as $\mathcal{X} = \bigcup_{i=1}^{\alpha} \mathcal{X}(i)$. Our objective is to identify β representative images from each quality interval, characterized by minimal variability in their MOS scores, enhancing the consistency of our experimental dataset. Images with high variability in human ratings are deemed less suitable for evaluating the performance of LLMs due to the potential introduction of noise and biases. For each interval $\mathcal{X}(i)$, we aim to select a subset $\mathcal{A}(i) \subseteq \mathcal{X}(i)$, where the size of $\mathcal{A}(i)$ is β . This selection criterion is formalized through the following optimization problem:

$$\mathcal{A}(i) = \arg \min_{\mathcal{A} \subseteq \mathcal{X}(i), |\mathcal{A}|=\beta} \sum_{x \in \mathcal{A}} \sigma(x)^2, \quad (4)$$

where $\sigma(x)^2$ denotes the variance of the MOS score for image x , serving as a quantitative measure of rating consistency. As such, the full set of anchor images can be achieved by $\mathcal{A} = \bigcup_{i=1}^{\alpha} \mathcal{A}(i)$

Probability Matrix Construction. Based on the selected anchor images and visual quality comparator, we first construct probability matrix $P_a \in \mathbb{R}^{m \times m}$ for the anchor images as follows:

$$P_a = \begin{bmatrix} P(a^{(1)}, a^{(1)}) & P(a^{(1)}, a^{(2)}) & \dots & P(a^{(1)}, a^{(m)}) \\ P(a^{(2)}, a^{(1)}) & P(a^{(2)}, a^{(2)}) & \dots & P(a^{(2)}, a^{(m)}) \\ \vdots & \vdots & \ddots & \vdots \\ P(a^{(m)}, a^{(1)}) & P(a^{(m)}, a^{(2)}) & \dots & P(a^{(m)}, a^{(m)}) \end{bmatrix} \quad (5)$$

Notably, each element $P(a^{(i)}, a^{(j)}) = 1 - P(a^{(j)}, a^{(i)})$ and $P(a^{(i)}, a^{(i)}) = 0.5$. Then, the test image $x^{(m+1)}$ is compared with all anchor images. We use $b = [P(a^{(1)}, x^{(m+1)}), P(a^{(2)}, x^{(m+1)}), \dots, P(a^{(m)}, x^{(m+1)})]$ to denote the resultant vector. Therefore, we finally form the complete probability matrix $P \in \mathbb{R}^{(m+1) \times (m+1)}$ for the anchor and test images as $P = \begin{bmatrix} P_a & b \\ (1-b) & 0.5 \end{bmatrix}$.

Quality Score Estimation. Once obtaining the probability matrix, we compute the quality scores using MAP estimation under Thurstone’s Case V model [52]. It is expressed as a convex optimization problem [49]:

$$\arg \max_{\hat{q}} P_{ij} \log(\Phi(\hat{q}^{(i)} - \hat{q}^{(j)})) - \sum_i \frac{\hat{q}^{(i)}}{2}, \quad \text{s.t.} \quad \sum_i \hat{q}^{(i)} = 0, \quad (6)$$

where $\Phi(\cdot)$ is the standard Normal cumulative distribution function, and $\hat{q}^{(m+1)}$ represents the quality score of the test image.

4 Experiments

4.1 Experimental Setups

IQA Datasets. We conduct comprehensive experiments across six standard IQA datasets. These datasets are categorized based on the type of distortions they contain: synthetic distortions are featured in LIVE [53], CSIQ [24], and KADID-10k [26]; realistic distortions are present in BID [25], LIVE Challenge (denoted as CLIVE) [54], and KonIQ-10K [7]. More details regarding these IQA datasets can be found in the Appendix B. For our experiments, we utilize the ten splits provided by LIQE⁴, allocating 70% of images from each dataset for training, 10% for validation, and the remaining 20% for testing. We combine the training and validation sets in our experiments since **Compare2Score** are evaluated at the last optimization iteration without any fine-tuning of the model parameters [12, 46]. For datasets with synthetic distortions, it strictly maintains content independence by splitting datasets using reference images [10]. The median of the Spearman’s rank correlation coefficient (SRCC) and Pearson linear correlation coefficient (PLCC) across the ten splits are reported in the tables.

Implementation Details. **Compare2Score** utilizes the advanced mPLUG-Owl2 model [20] for its architecture, leveraging a pre-trained CLIP-ViT-L14 as the vision encoder [55] and LLaMA2-7B [51] as the LLM decoder. To train the model, we generate 180,000 image pairs and optimize the whole architecture with the GPT loss [56], which computes cross-entropy between the predicted logits and ground-truth labels. Training is conducted with a batch size of 64 across all datasets, a fixed learning rate of 2×10^{-5} , and spans two epochs. This process requires seven NVIDIA A40 GPUs to meet the computational load. During inference, a single NVIDIA RTX3090 GPU is sufficient for executing the soft comparison (Sec. 3.4). Furthermore, to obtain the anchor images, we divide the training set of the KonIQ-10k into five ($\alpha = 5$) quality intervals based on their MOSs [57], from which we select one ($\beta = 1$) representative anchor image per interval using Eqn. (4).

Baselines. We compare the performance of the proposed **Compare2Score** with the following state-of-the-art methods, which include (1) three opinion-unaware NR-IQA models: NIQE [2], ILNIQE [3], and Ma19 [58]; (2) six learning-to-regress NR-IQA models: PaQ2PiQ [6], KonCept [7], MUSIQ [59], DBCNN [4], HyperIQA [8], and TreS [11]; (3) two learning-to-rank NR-IQA models: UNIQUE [17] and LIQE [10]; (4) one LMM-based NR-IQA model: Q-Align [12]. All methods are compared with the same testing sets across ten splits. The UNIQUE, LIQE, and Q-Align are jointly trained on the above six datasets, respectively. The remaining methods are separately trained on each individual dataset if necessary.

Table 1: Performance comparison in terms of median SRCC and PLCC on six IQA datasets. The methods are jointly trained with a mixture of six datasets are represented in italics.

Method	LIVE [53]		CSIQ [24]		KADID-10k [26]		BID [25]		CLIVE [54]		KonIQ-10k [7]	
	SRCC	PLCC	SRCC	PLCC	SRCC	PLCC	SRCC	PLCC	SRCC	PLCC	SRCC	PLCC
NIQE [2]	0.908	0.904	0.631	0.719	0.389	0.442	0.573	0.618	0.446	0.507	0.415	0.438
ILNIQE [3]	0.887	0.894	0.808	0.851	0.565	0.611	0.548	0.494	0.469	0.518	0.509	0.534
Ma19 [58]	0.922	0.923	0.926	0.929	0.465	0.501	0.373	0.399	0.336	0.405	0.360	0.398
PaQ2PiQ [6]	0.544	0.558	0.697	0.766	0.403	0.448	0.719	0.700	0.732	0.755	0.722	0.716
KonCept [7]	0.673	0.619	0.631	0.645	0.503	0.515	0.816	0.825	0.778	0.799	0.911	0.924
MUSIQ [59]	0.837	0.818	0.697	0.766	0.572	0.584	0.744	0.774	0.785	0.828	0.915	0.937
DBCNN [4]	0.963	0.966	0.940	0.954	0.878	0.878	0.864	0.883	0.835	0.854	0.864	0.868
HyperIQA [8]	0.966	0.968	0.934	0.946	0.872	0.869	0.848	0.868	0.855	0.878	0.900	0.915
TreS [11]	0.965	0.963	0.902	0.923	0.881	0.879	0.853	0.871	0.846	0.877	0.907	0.924
<i>UNIQUE [17]</i>	0.961	0.952	0.902	0.921	0.884	0.885	0.852	0.875	0.854	0.884	0.895	0.900
<i>LIQE [10]</i>	0.970	0.951	0.936	0.939	0.930	0.931	0.875	0.900	0.904	0.910	0.919	0.908
<i>Q-Align [12]</i>	0.913	0.919	0.915	0.936	0.869	0.927	0.904	0.920	0.931	0.921	0.935	0.934
Compare2Score	0.972	0.969	0.950	0.943	0.952	0.939	0.919	0.939	0.914	0.928	0.931	0.939

4.2 Main Results

Performance under Intra-Dataset Setting. Table 1 shows the results of media SRCC and PLCC across ten sessions. It is clear that **Compare2Score** outperforms the competing methods on both

⁴https://github.com/zwx8981/LIQE/tree/main/IQA_Database

Table 2: SRCC results on the three IQA datasets under the cross-dataset setup. The methods are jointly trained with a mixture of six datasets are represented in italics.

Method	TID2013 [24]	SPAQ [60]	AGIQA-3K [61]
NIQE [2]	0.314	0.578	0.562
PaQ2PiQ [6]	0.423	0.823	0.502
MUSIQ [59]	0.584	0.853	0.629
DBCNN [4]	0.686	0.412	0.654
HyperIQA [8]	-	-	0.629
Tres [62]	-	-	0.646
<i>UNIQUE</i> [17]	0.768	0.838	0.666
<i>LIQE</i> [10]	0.811	0.881	0.721
<i>Q-Align</i> [12]	0.801	0.813	0.725
Compare2Score	0.823	0.906	0.730

Table 3: SRCC results of probability matrix and count matrix on four IQA datasets. Prob. stands for probability.

Method	Matrix	LIVE [53]	CSIQ [24]	BID [25]	CLIVE [54]
IDEFICS [19]	Count	0.157	0.008	0.015	0.206
	Prob.	0.363	0.044	0.227	0.385
LLaVA-1.5 [21]	Count	0.214	0.148	0.122	0.015
	Prob.	0.386	0.555	0.361	0.292
mPLUG-Owl2 [20]	Count	0.408	0.013	0.217	0.221
	Prob.	0.449	0.129	0.551	0.355
XComposer-VL-2 [22]	Count	0.199	0.145	0.206	0.332
	Prob.	0.323	0.301	0.598	0.455
Co-Instruct [46]	Count	0.582	0.569	0.820	0.694
	Prob.	0.822	0.768	0.866	0.768
Compare2Score	Count	0.888	0.875	0.778	0.816
	Prob.	0.974	0.942	0.921	0.934

synthetic and realistic distortions, demonstrating the reliability of the paired comparison strategy can be smoothly extended to the LMM. While Q-Align [12] is another LMM-based model, it presents inferior performance on the synthetically distorted datasets [53, 24, 26]. The main reason may be the perceptual scale ambiguity across different IQA datasets. The pairwise learning-to-rank approach employed by UNIQUE [17] and LIQE [10] achieves competitive performance against models [4, 8, 11] trained individually, which further validates the effectiveness of using relative ranking information to mix different IQA datasets. Additionally, the opinion-unaware models exhibit subpar performance on the realistic distortions, suffering the potential overfitting issue to the traditional synthetic distortions [53, 24]. Furthermore, though the learning-to-regress models are able to achieve promising performance on individual datasets with unique parameters, each dataset requires a unique set of parameters that hinder the practicality of such models in the real world.

Performance under Cross-Dataset Setting. To assess the generalization capability of **Compare2Score** against competitive NR-IQA models, we conduct the cross-distortion experiments with three challenging unseen IQA datasets: TID2013 [63], SPAQ [60], and AGIQA-3K [61]. In particular, TID2013 contains 24 distortion types, most of which are different from distortions in the training datasets. SPAQ consists of 11, 125 images captured by 66 smartphones, undergoing abundant realistic distortions. The images in AGIQA-3K are generated by six advanced text-to-image generative models, which cast significant challenges to the NR-IQA models. The results are summarized in Table 2, from which we can observe that **Compare2Score** demonstrates the strongest generalization capability across synthetic, realistic, and generative distortions. We believe the robustness of the proposed model benefits from 1) the high capacity of the LMM-based model, 2) the proposed soft comparison mechanism, and 3) the joint training on multiple datasets.

Performance of Probability Matrix and Count Matrix. In order to demonstrate the efficacy of our proposed soft comparison method, we conducted an evaluation comparing the newly designed probability matrix against the traditional count matrix [49] with five state-of-the-art LMMs, including IDEFICS [19], LLaVA-1.5 [21], mPLUG-Owl2 [20], XComposer-VL-2 [22], and Co-Instruct [46]. Detailed information about these models is available in the Appendix C. The comparative results are detailed in Table 3. The results reveal that our probability matrix not only enhances the performance of **Compare2Score** but also significantly zero-shot the IQA performance across five open-source LMMs [19, 21, 20, 22, 46]. This consistent outperformance highlights the robustness and utility of the soft comparison approach in diverse IQA contexts.

Performance of Prediction Accuracy. We further compare the prediction accuracy of paired comparison results of **Compare2Score** to five open-source LMMs [19, 21, 20, 22, 46]. As shown in Table 4, **Compare2Score** significantly surpasses these advanced open-source LMMs, providing high accuracy of quantitative outputs. Notably, Co-Instruct achieves competitive accuracy across the six IQA datasets, benefiting from a specialized visual quality comparison training corpus. The models (e.g., IDEFICS, LLaVA-1.5, mPLUG-Owl2, and XComposer-VL-2) rely on high-level instruction-tuning datasets showing poor performance in terms of prediction accuracy, suggesting an inferior quality comparison capability of these LMMs.

Table 4: Performance comparison in terms of prediction accuracy on six IQA datasets. The best results are highlighted in boldface.

Method	LIVE [53]	CSIQ [24]	KADID-10k [26]	BID [25]	CLIVE [54]	KonIQ-10k [7]
IDEFICS [19]	0.125	0.669	0.500	0.523	0.146	0.727
LLaVA-1.5 [21]	0.170	0.544	0.600	0.579	0.074	0.455
mPLUG-Owl2 [20]	0.484	0.394	0.302	0.613	0.407	0.273
XComposer-VL-2 [22]	0.045	0.662	0.672	0.648	0.067	0.059
Co-Instruct [46]	0.672	0.426	0.391	0.695	0.718	0.849
Compare2Score	0.849	0.720	0.870	0.861	0.788	0.858

Table 5: SRCC results for **Compare2Score** using anchor images from KonIQ-10k [7], KADID-10k [26], and AGIQA-3K [61].

Dataset	KonIQ-10k [7]	KADID-10k [26]	AGIQA-3K [61]
LIVE [53]	0.972	0.968	0.975
CSIQ [24]	0.950	0.947	0.946
KADID-10k [26]	0.952	0.957	0.944
BID [25]	0.919	0.914	0.916
CLIVE [54]	0.914	0.912	0.915
KonIQ-10k [7]	0.939	0.931	0.929

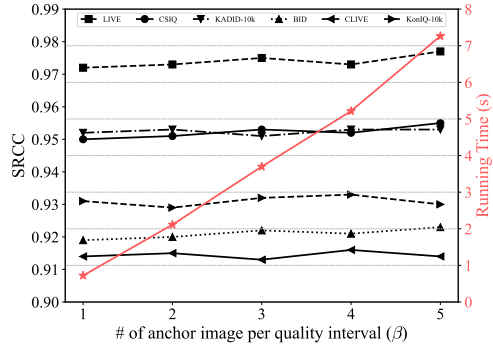


Figure 4: Comparisons of SRCC results and running time with different numbers of anchor image per quality interval (β).

4.3 Ablation Studies

Impact of the Source of Anchor Images. Although KonIQ-10k [7] serves as the default source for anchor images, we demonstrate the robustness of our results across diverse sources of anchor images. Utilizing the same anchor image selection strategy outlined in Eqn. (4), we selected anchor images from three distinct datasets: KADID-10k [26], featuring synthetic distortions; KonIQ-10k [7], with realistic distortions; and AGIQA-3K [61], containing generative distortions. As shown in Table 5, **Compare2Score** consistently shows superior performance across all IQA datasets, showing remarkable robustness to the varying types of distortions of the anchor images. The anchor images selected from the three datasets are shown in Appendix E.

Impact of the Number of Anchor images. The number of anchor images within each quality interval (β in Eqn. (4)) crucially affects the efficacy of **Compare2Score**. We systematically explore the influence of β and present the SRCC results and running times in Fig. 4. Notably, all experiments were carried out on the same testing platform equipped with an NVIDIA RTX3090 GPU. The results illustrated in Fig. 4 indicate that increasing the number of anchor images does not enhance performance across the evaluated IQA datasets. $\beta = 1$ suffices for achieving promising and state-of-the-art performance. In addition, it is expected that the average running time (red line in Fig. 4) linearly increases as β becomes large. As a result, $\beta = 1$ has been set as the optimal configuration to achieve a practical balance between model efficiency and computational expense. The ablation experiment of the anchor image selection method is included in the Appendix D.

5 Conclusion and Discussion

In this paper, we introduced **Compare2Score**, a novel NR-IQA model utilizing LMM to bridge the gap between discrete comparative levels and continuous quality scores. By using the robust capabilities of LMMs to interpret and integrate complex textual and visual inputs, our model excels in translating scaled-up comparative instructions into reliable, human-like quality assessments. We propose an innovative soft comparison method that effectively and efficiently converts discrete textual responses to continuous quality scores. Extensive validation on standard IQA datasets demonstrates that the proposed model significantly outperforms existing NR-IQA models across different distortion scenarios. Moreover, our probability-matrix-based improves both our model and general-purpose LMMs, showcasing the broad applicability and intrinsic effectiveness of our methods.

References

- [1] Zhou Wang and Alan C. Bovik. *Modern Image Quality Assessment*. Morgan & Claypool, 2006.
- [2] Anish Mittal, Rajiv Soundararajan, and Alan C. Bovik. Making a “completely blind” image quality analyzer. *IEEE Signal Processing Letters*, 20(3):209–212, Mar. 2013.
- [3] Lin Zhang, Lei Zhang, and Alan C. Bovik. A feature-enriched completely blind image quality evaluator. *IEEE Transactions on Image Processing*, 24(8):2579–2591, Aug. 2015.
- [4] Weixia Zhang, Kede Ma, Jia Yan, Dexiang Deng, and Zhou Wang. Blind image quality assessment using a deep bilinear convolutional neural network. *IEEE Transactions on Circuits and Systems for Video Technology*, 30(1):36–47, Jan. 2020.
- [5] Baoliang Chen, Lingyu Zhu, Chenqi Kong, Hanwei Zhu, Shiqi Wang, and Zhu Li. No-reference image quality assessment by hallucinating pristine features. *IEEE Transactions on Image Processing*, 31:6139–6151, 2022.
- [6] Zhenqiang Ying, Haoran Niu, Praful Gupta, Dhruv Mahajan, Deepti Ghadiyaram, and Alan C. Bovik. From patches to pictures (PaQ-2-PiQ): Mapping the perceptual space of picture quality. In *IEEE Conference on Computer Vision and Pattern Recognition*, pages 3572–3582, 2020.
- [7] Vlad Hosu, Hanhe Lin, Tamas Sziranyi, and Dietmar Saupe. KonIQ-10k: An ecologically valid database for deep learning of blind image quality assessment. *IEEE Transactions on Image Processing*, 29:4041–4056, Jan. 2020.
- [8] Shaolin Su, Qingsen Yan, Yu Zhu, Cheng Zhang, Xin Ge, Jinqiu Sun, and Yanning Zhang. Blindly assess image quality in the wild guided by a self-adaptive hyper network. In *IEEE Conference on Computer Vision and Pattern Recognition*, pages 3667–3676, 2020.
- [9] Jianyi Wang, Kelvin CK Chan, and Chen Change Loy. Exploring CLIP for assessing the look and feel of images. *CoRR*, abs/2207.12396, 2022.
- [10] Weixia Zhang, Guangtao Zhai, Ying Wei, Xiaokang Yang, and Kede Ma. Blind image quality assessment via vision-language correspondence: A multitask learning perspective. In *IEEE Conference on Computer Vision and Pattern Recognition*, pages 14071–14081, 2023.
- [11] S. Alireza Golestaneh, Saba Dadsetan, and Kris M. Kitani. No-reference image quality assessment via transformers, relative ranking, and self-consistency. In *IEEE Winter Conference on Applications of Computer Vision*, pages 1220–1230, 2022.
- [12] Haoning Wu, Zicheng Zhang, Weixia Zhang, Chaofeng Chen, Liang Liao, Chunyi Li, Yixuan Gao, Annan Wang, Erli Zhang, Wenxiu Sun, et al. Q-Align: Teaching LMMs for visual scoring via discrete text-defined levels. *CoRR*, abs/2312.17090, 2023.
- [13] Hancheng Zhu, Leida Li, Jinjian Wu, Weisheng Dong, and Guangming Shi. MetaIQA: Deep meta-learning for no-reference image quality assessment. In *IEEE Conference on Computer Vision and Pattern Recognition*, pages 14131–14140, 2020.
- [14] Baoliang Chen, Haoliang Li, Hongfei Fan, and Shiqi Wang. No-reference screen content image quality assessment with unsupervised domain adaptation. *IEEE Transactions on Image Processing*, 30:5463–5476, 2021.
- [15] Subhadeep Roy, Shankhanil Mitra, Soma Biswas, and Rajiv Soundararajan. Test time adaptation for blind image quality assessment. In *IEEE International Conference on Computer Vision*, pages 16742–16751, 2023.
- [16] Zhihua Wang, Qiuping Jiang, Shanshan Zhao, Wensen Feng, and Weisi Lin. Deep blind image quality assessment powered by online hard example mining. *IEEE Transactions on Multimedia*, to appear 2023.
- [17] Weixia Zhang, Kede Ma, Guangtao Zhai, and Xiaokang Yang. Uncertainty-aware blind image quality assessment in the laboratory and wild. *IEEE Transactions on Image Processing*, 30:3474–3486, Mar. 2021.
- [18] OpenAI. GPT-4V(ision) system card. https://cdn.openai.com/papers/GPTV_System_Card.pdf/, 2023.
- [19] Hugging Face. Introducing IDEFICS: An open reproduction of state-of-the-art visual language model. <https://huggingface.co/blog/idefics/>, 2023.
- [20] Qinghao Ye, Haiyang Xu, Jiabo Ye, Ming Yan, Haowei Liu, Qi Qian, Ji Zhang, Fei Huang, and Jingren Zhou. mPLUG-Owl2: Revolutionizing multi-modal large language model with modality collaboration. *CoRR*, abs/2311.04257, 2023.
- [21] Haotian Liu, Chunyuan Li, Yuheng Li, and Yong Jae Lee. Improved baselines with visual instruction tuning. *CoRR*, abs/2310.03744, 2023.
- [22] Xiaoyi Dong, Pan Zhang, Yuhang Zang, Yuhang Cao, Bin Wang, Linke Ouyang, Xilin Wei, Songyang Zhang, Haodong Duan, Maosong Cao, et al. InternLM-XComposer2: Mastering free-form text-image composition and comprehension in vision-language large model. *CoRR*, abs/2401.16420, 2024.

- [23] Haotian Liu, Chunyuan Li, Qingyang Wu, and Yong Jae Lee. Visual instruction tuning. *Advances in Neural Information Processing Systems*, pages 34892–34916, 2024.
- [24] Eric C. Larson and Damon M. Chandler. Most apparent distortion: Full-reference image quality assessment and the role of strategy. *Journal of Electronic Imaging*, 19(1):1–21, Jan. 2010.
- [25] Alexandre Ciancio, A. L. N. T. Targino da Costa, E. A. B. da Silva, Amir Said, Ramin Samadani, and Pere Obrador. No-reference blur assessment of digital pictures based on multifeature classifiers. *IEEE Transactions on Image Processing*, 20(1):64–75, Jan. 2011.
- [26] Hanhe Lin, Vlad Hosu, and Dietmar Saupe. KADID-10k: A large-scale artificially distorted IQA database. In *International Conference on Quality of Multimedia Experience*, pages 1–3, 2019.
- [27] Rafał K Mantiuk, Anna Tomaszewska, and Radosław Mantiuk. Comparison of four subjective methods for image quality assessment. *Computer Graphics Forum*, 31(8):2478–2491, 2012.
- [28] Anish Mittal, Anush K. Moorthy, and Alan C. Bovik. No-reference image quality assessment in the spatial domain. *IEEE Transactions on Image Processing*, 21(12):4695–4708, Dec. 2012.
- [29] Jingtao Xu, Peng Ye, Qiaohong Li, Haiqing Du, Yong Liu, and David Doermann. Blind image quality assessment based on high order statistics aggregation. *IEEE Transactions on Image Processing*, 25(9):4444–4457, Sep. 2016.
- [30] Qingbo Wu, Hongliang Li, King N Ngan, and Kede Ma. Blind image quality assessment using local consistency aware retriever and uncertainty aware evaluator. *IEEE Transactions on Circuits and Systems for Video Technology*, 28(9):2078–2089, 2017.
- [31] Ke Gu, Guangtao Zhai, Xiaokang Yang, and Wenjun Zhang. Using free energy principle for blind image quality assessment. *IEEE Transactions on Multimedia*, 17(1):50–63, Jan. 2015.
- [32] Pavan C. Madhusudana, Neil Birkbeck, Yilin Wang, Balu Adsumilli, and Alan C. Bovik. Image quality assessment using contrastive learning. *IEEE Transactions on Image Processing*, 31:4149–4161, Jun. 2022.
- [33] Chaofeng Chen, Jiadi Mo, Jingwen Hou, Haoning Wu, Liang Liao, Wenxiu Sun, Qiong Yan, and Weisi Lin. TOPIQ: A top-down approach from semantics to distortions for image quality assessment. *IEEE Transactions on Image Processing*, to appear 2024.
- [34] Kede Ma, Wentao Liu, Kai Zhang, Zhengfang Duanmu, Zhou Wang, and Wangmeng Zuo. End-to-end blind image quality assessment using deep neural networks. *IEEE Transactions on Image Processing*, 27(3):1202–1213, 2017.
- [35] B. T. ITU-R. Methodology for the subjective assessment of the quality of television pictures. <https://www.itu.int/rec/R-REC-BT.500>, 2002.
- [36] Fei Gao, Dacheng Tao, Xinbo Gao, and Xuelong Li. Learning to rank for blind image quality assessment. *IEEE Transactions on Neural Networks and Learning Systems*, 26(10):2275–2290, Oct. 2015.
- [37] Xialei Liu, Joost van de Weijer, and Andrew D. Bagdanov. RankIQA: Learning from rankings for no-reference image quality assessment. In *IEEE International Conference on Computer Vision*, pages 1040–1049, 2017.
- [38] Kede Ma, Wentao Liu, Tongliang Liu, Zhou Wang, and Dacheng Tao. dipIQ: Blind image quality assessment by learning-to-rank discriminable image pairs. *IEEE Transactions on Image Processing*, 26(8):3951–3964, Aug. 2017.
- [39] Haoning Wu, Zicheng Zhang, Erli Zhang, Chaofeng Chen, Liang Liao, Annan Wang, Kaixin Xu, Chunyi Li, Jingwen Hou, Guangtao Zhai, et al. Q-Instruct: Improving low-level visual abilities for multi-modality foundation models. *CoRR*, abs/2311.06783, 2023.
- [40] Hanwei Zhu, Xiangjie Sui, Baoliang Chen, Xuelin Liu, Peilin Chen, Yuming Fang, and Shiqi Wang. 2AFC prompting of large multimodal models for image quality assessment. *CoRR*, abs/2402.01162, 2024.
- [41] Zicheng Zhang, Haoning Wu, Erli Zhang, Guangtao Zhai, and Weisi Lin. A benchmark for multi-modal foundation models on low-level vision: from single images to pairs. *CoRR*, abs/2402.07116, 2024.
- [42] Tianhe Wu, Kede Ma, Jie Liang, Yujiu Yang, and Lei Zhang. A comprehensive study of multimodal large language models for image quality assessment. *CoRR*, abs/2403.10854, 2024.
- [43] Zicheng Zhang, Haoning Wu, Zhongpeng Ji, Chunyi Li, Erli Zhang, Wei Sun, Xiaohong Liu, Xiongkuo Min, Fengyu Sun, Shangling Jui, et al. Q-Boost: On visual quality assessment ability of low-level multi-modality foundation models. *CoRR*, abs/2312.15300, 2023.
- [44] Zhipeng Huang, Zhizheng Zhang, Yiting Lu, Zheng-Jun Zha, Zhibo Chen, and Baining Guo. VisualCritic: Making LMMs perceive visual quality like humans. *CoRR*, abs/2403.12806, 2024.
- [45] Zhiyuan You, Zheyuan Li, Jinjin Gu, Zhenfei Yin, Tianfan Xue, and Chao Dong. Depicting beyond scores: Advancing image quality assessment through multi-modal language models. *CoRR*, abs/2312.08962, 2023.

- [46] Haoning Wu, Hanwei Zhu, Zicheng Zhang, Erli Zhang, Chaofeng Chen, Liang Liao, Chunyi Li, Annan Wang, Wenxiu Sun, Qiong Yan, et al. Towards open-ended visual quality comparison. *CoRR*, abs/2402.16641, 2024.
- [47] Haoning Wu, Zicheng Zhang, Erli Zhang, Chaofeng Chen, Liang Liao, Annan Wang, Chunyi Li, Wenxiu Sun, Qiong Yan, Guangtao Zhai, et al. Q-Bench: A benchmark for general-purpose foundation models on low-level vision. *CoRR*, abs/2309.14181, 2023.
- [48] Zhengfang Duanmu, Wentao Liu, Zhongling Wang, and Zhou Wang. Quantifying visual image quality: A bayesian view. *Annual Review of Vision Science*, 7(1):437–464, 2021.
- [49] Kristi Tsukida and Maya R Gupta. How to analyze paired comparison data, Technical Report UWEETR-2011-0004, University of Washington, 2011.
- [50] Sheskin David J. *Handbook of Parametric and Nonparametric Statistical Procedures*. CRC Press, 2004.
- [51] Hugo Touvron, Louis Martin, Kevin Stone, Peter Albert, Amjad Almahairi, Yasmine Babaei, Nikolay Bashlykov, Soumya Batra, Prajjwal Bhargava, Shruti Bhosale, et al. LLaMA 2: Open foundation and fine-tuned chat models. *CoRR*, abs/2307.09288, 2023.
- [52] Louis L. Thurstone. A law of comparative judgment. *Psychological Review*, 34:273–286, Jul. 1927.
- [53] Hamid R. Sheikh, Muhammad F. Sabir, and Alan C. Bovik. A statistical evaluation of recent full reference image quality assessment algorithms. *IEEE Transactions on Image Processing*, 15(11):3440–3451, Nov. 2006.
- [54] Deepti Ghadiyaram and Alan C. Bovik. Massive online crowdsourced study of subjective and objective picture quality. *IEEE Transactions on Image Processing*, 25(1):372–387, Jan. 2016.
- [55] Alec Radford, Jong Wook Kim, Chris Hallacy, Aditya Ramesh, Gabriel Goh, Sandhini Agarwal, Girish Sastry, Amanda Askell, Pamela Mishkin, Jack Clark, Gretchen Krueger, and Ilya Sutskever. Learning transferable visual models from natural language supervision. In *International Conference on Machine Learning*, pages 8748–8763, 2021.
- [56] Alec Radford, Jeffrey Wu, Rewon Child, David Luan, Dario Amodei, Ilya Sutskever, et al. Language models are unsupervised multitask learners. *OpenAI Blog*, 1(8):9, 2019.
- [57] VQEG. Final report from the video quality experts group on the validation of objective models of video quality assessment, 2000.
- [58] Kede Ma, Xuelin Liu, Yuming Fang, and Eero P. Simoncelli. Blind image quality assessment by learning from multiple annotators. In *IEEE International Conference on Image Processing*, pages 2344–2348, 2019.
- [59] Junjie Ke, Qifei Wang, Yilin Wang, Peyman Milanfar, and Feng Yang. MUSIQ: Multi-scale image quality transformer. In *IEEE International Conference on Computer Vision*, pages 5148–5157, 2021.
- [60] Yuming Fang, Hanwei Zhu, Yan Zeng, Kede Ma, and Zhou Wang. Perceptual quality assessment of smartphone photography. In *IEEE Conference on Computer Vision and Pattern Recognition*, pages 3677–3686, 2020.
- [61] Chunyi Li, Zicheng Zhang, Haoning Wu, Wei Sun, Xiongkuo Min, Xiaohong Liu, Guangtao Zhai, and Weisi Lin. AGIQA-3K: An open database for ai-generated image quality assessment. *IEEE Transactions on Circuits and Systems for Video Technology*, to appear 2023.
- [62] Tal Golan, Prashant C Raju, and Nikolaus Kriegeskorte. Controversial stimuli: Pitting neural networks against each other as models of human cognition. *Proceedings of the National Academy of Sciences*, 117(47):29330–29337, 2020.
- [63] Ponomarenko Nikolay, Jin Lina, Ieremeiev Oleg, Lukin Vladimir, Egiazarian Karen, Astola Jaakko, Vozel Benoit, Chehdi Kacem, Carli Marco, Battisti Federica, and C.-C. Jay Kuo. Image database TID2013: Peculiarities, results and perspectives. *Signal Processing: Image Communication*, 30:57–77, Jan. 2015.
- [64] Bart Thomee, David A Shamma, Gerald Friedland, Benjamin Elizalde, Karl Ni, Douglas Poland, Damian Borth, and Li-Jia Li. YFCC100M: The new data in multimedia research. *Communications of the ACM*, 59(2):64–73, 2016.
- [65] Tao Xu, Pengchuan Zhang, Qiuyuan Huang, Han Zhang, Zhe Gan, Xiaolei Huang, and Xiaodong He. AttnGan: Fine-grained text to image generation with attentional generative adversarial networks. In *IEEE Conference on Computer Vision and Pattern Recognition*, pages 1316–1324, 2018.
- [66] Aditya Ramesh, Prafulla Dhariwal, Alex Nichol, Casey Chu, and Mark Chen. Hierarchical text-conditional image generation with CLIP latents. *CoRR*, abs/2204.06125, 2022.
- [67] Alex Nichol, Prafulla Dhariwal, Aditya Ramesh, Pranav Shyam, Pamela Mishkin, Bob McGrew, Ilya Sutskever, and Mark Chen. GLIDE: Towards photorealistic image generation and editing with text-guided diffusion models. *CoRR*, abs/2112.10741, 2021.
- [68] David Holz. Midjourney. url = <https://www.midjourney.com/>, 2023.

- [69] Robin Rombach, Andreas Blattmann, Dominik Lorenz, Patrick Esser, and Björn Ommer. High-resolution image synthesis with latent diffusion models. In *IEEE Conference on Computer Vision and Pattern Recognition*, pages 10684–10695, 2022.
- [70] Robin Rombach, Andreas Blattmann, and Björn Ommer. Text-guided synthesis of artistic images with retrieval-augmented diffusion models. *CoRR*, abs/2207.13038, 2022.
- [71] Anas Awadalla, Irena Gao, Josh Gardner, Jack Hessel, Yusuf Hanafy, Wanrong Zhu, Kalyani Marathe, Yonatan Bitton, Samir Gadre, Shiori Sagawa, et al. Openflamingo: An open-source framework for training large autoregressive vision-language models. *CoRR*, abs/2308.01390, 2023.
- [72] Hugo Laurençon, Lucile Saulnier, Léo Tronchon, Stas Bekman, Amanpreet Singh, Anton Lozhkov, Thomas Wang, Siddharth Karamcheti, Alexander M. Rush, Douwe Kiela, Matthieu Cord, and Victor Sanh. OBELICS: An open web-scale filtered dataset of interleaved image-text documents. *CoRR*, abs/2306.16527, 2023.
- [73] Wei-Lin Chiang, Zhuohan Li, Zi Lin, Ying Sheng, Zhanghao Wu, Hao Zhang, Lianmin Zheng, Siyuan Zhuang, Yonghao Zhuang, Joseph E Gonzalez, et al. Vicuna: An open-source chatbot impressing GPT-4 with 90%* chatgpt quality. See <https://vicuna.lmsys.org> (accessed 14 April 2023), 2(3):6, 2023.
- [74] Zheng Cai, Maosong Cao, Haojiong Chen, Kai Chen, Keyu Chen, Xin Chen, Xun Chen, Zehui Chen, Zhi Chen, Pei Chu, et al. Internlm2 technical report. *CoRR*, abs/2403.17297, 2024.

A Broader Impacts

The social impact of our research on an LMM-based NR-IQA model is substantial. By integrating diverse IQA datasets more effectively, this model promotes enhanced consistency and reliability in image quality evaluations across different real-world applications. Particularly in fields such as image processing, computer vision, and computer graphics, the ability to accurately assess image quality is paramount. As these sectors increasingly rely on visual content, ensuring high-quality, reliable assessments directly influences consumer satisfaction and operational efficiency. Moreover, by advancing the capabilities of LMMs in interpreting and integrating complex, varied data sources, our approach not only improves the precision of image quality scoring systems but also contributes to the broader adoption of responsible AI technologies. This innovation holds promise for setting new benchmarks in the automation of quality control, fostering trust and dependability in digital media and related technologies, ultimately benefiting society at large.

B More Details on IQA Datasets

The details of the utilized IQA datasets are described as follows.

- **LIVE [53]:** The LIVE database contains 29 reference images and 779 distorted images with the 5 distortions, including JPEG compression, JPEG2000 compression, additive white Gaussian noise, Gaussian blur, and fast-fading transmission distortion. The single-stimulus continuous quality rating is used to collect human opinions. The difference MOSs (DMOS) spread from 0 to 100.
- **CSIQ [24]:** The CSIQ database contains 30 reference images and 866 distorted images with 6 distortions of JPEG compression, JPEG2000 compression, Gaussian blur, Gaussian white noise, Gaussian pink noise, and contrast change. The subjective testing method is the single-stimulus absolute category rating. The DMOSs span from 0 to 1.
- **TID2013 [24]:** The TID2013 database contains 25 reference images and 3,000 distorted images with 24 distortions such as noise (*e.g.*, additive Gaussian, masked, high frequency noise), compression (*e.g.*, JPEG, JPEG2000 compression), contrast change, etc. Paired comparison is the subjective user study methodology. The MOSs spread from 0 to 9.
- **KADID-10k [26]:** The KADID-10k database contains 81 reference images and 10,125 distorted images by adding 25 distortion types with 5 distortion levels such as blur, color distortions, noise, spatial distortions, etc. The subjective testing method is the double-stimulus continuous quality rating by crowdsourcing. The DMOSs range from 1 to 5.
- **BID [25]:** The BID database collects a total of 586 realistic distortion images with professional digital single-lens reflex cameras. The single-stimulus continuous quality rating is applied to collect human opinions. The MOSs range from 0 to 5.
- **CLIVE [54]:** The LIVE Challenge (denoted as CLIVE) database contains 1,162 images with realistic distortions captured by multiple mobile devices. The subjective experiment methodology is the single-stimulus method with crowdsourcing. The MOSs range from 0 to 100.
- **KonIQ-10k [7]:** The KonIQ-10k database consists of 10,073 images with abundant realistic distortions. Those are selected from the YFCC100M database [64]. Single-stimulus absolute category rating is the method of subjective testing. The MOSs range from 1 to 5.
- **SPAQ [60]:** The SPAQ database consists of 11,125 in-the-wild pictures taken by 66 smartphones. Each picture is annotated with quality, attributes, and scene categories using the single-stimulus methodology. The MOSs range from 0 to 100.
- **AGIQA-3K [61]:** The AGIQA-3K consists of 2,982 AI-generated images derived from 6 advanced text-to-image generation models, which includes AttnGAN [65], DALLE2 [66], GLIDE [67], Midjourney [68], Stable Diffusion [69], and Stable Diffusion XL [70]. The single-stimulus continuous quality rating is used to collect human opinions. The MOSs range from 0 to 5.

Table 6: Overview of the baseline open-sourced LMMs compared with the proposed **Compare2Score**. MLP stands for the multilayer perceptron. MAM is the modality-adaptive module.

Model	Visual Model	Visual-Language Alignment	Language Model
LLaVA-1.5 [23]	CLIP-ViT-Large/14	MLP	Vicuna-7B
mPLUG-Owl2 [20]	CLIP-ViT-Large/14	MAM	LLaMA-7B
IDEFICS [19]	CLIP-ViT-Large/14	Cross-Attention	LLaMA-7B
XComposer-VL-2 [22]	CLIP-ViT-Large/14	Perceive Sampler	InternLM2-7B
Co-Instruct [46]	CLIP-ViT-Large/14	MAM	LLaMA-7B
Compare2Score	CLIP-ViT-Large/14	MAM	LLaMA-7B

C More Details on Competing LMMs

We evaluated the image quality prediction performance of the proposed **Compare2Score** against five LMMs: IDEFICS [19], LLaVA-1.5 [21], mPLUG-Owl2 [20], XComposer-VL-2 [22], and Co-Instruct [46]. Typically, LMMs consist of three core components: a modality encoder, a language model, and a modality interface for cross-modal interactions. Detailed information on these models is provided below and summarized in Table 6:

- **IDEFICS [19]:** The IDEFICS is based on the state-of-the-art visual language model Flamingo [71], encompassing the CLIP-ViT-L14 [55] as the vision encoder and LLaMA2-7B [51] as the large language model (LLM) backbone. It is trained on a vast dataset consisting of 141 million image-text documents and 353 million images [72].
- **LLaVA-1.5 [21]:** The LLaVA-1.5 model incorporates the pretrained CLIP-ViT-L14 [55] as the vision encoder, Vicuna-7B [73] as the LLM and an multilayer perceptron (MLP) as a visual-language connector. LLaVA-1.5 employs the single response formatting prompt in instruction-tuning as formatting control in order to regulate the answering layout.
- **mPLUG-Owl2 [20]:** The mPLUG-Owl2 model integrates the CLIP-ViT-L14 [55] for visual input and LLaMA2-7B [51] as the LLM, with a visual abstractor serving as the cross-modal interface. It emphasizes semantic consistency by decoupling visual-language representations into a shared semantic space, trained on multimodal instructions and image-text pairs.
- **XComposer-VL-2 [22]:** The Intern-XComposer-VL-2 (denoted as XComposer-VL-2) model utilizes the pretrained CLIP-ViT-L14 [55] as the vision encoder, the InternLM-2 [74] as the LLM, and a perceive sampler to connect modalities.
- **Co-Instruct [46]:** The Co-Instruct is built on the mPLUG-Owl2 framework [20], tailored for visual quality comparison using a specialized visual instruction dataset. It employs an image-text interleaved format to enhance the fidelity of information integration, making it highly effective for IQA tasks involving multiple images.

D Impact of the Anchor Selection Method

To evaluate the efficacy of the proposed anchor image selection method (referring to Eqn. (4)), we conducted a comparative analysis against a random selection strategy. The results are shown in Table 7, from which we can observe that **Compare2Score** surpasses random selection in enhancing model performance across six IQA datasets. This improvement indicates that selecting anchor images with low variability in human ratings is crucial, as high variability tends to introduce noise and biases, compromising the effectiveness of LMMs in performance evaluations. In addition, the randomly selected anchor images also demonstrated competitive performance compared with the state-of-the-art NR-IQA model in Table 1, which further verifies the effectiveness of the proposed **Compare2Score** framework.

E Illustrations of Anchor Images

Herein, we present the selected anchor images from KonIQ-10k [7], KADID-10k [26], and AGIQA-3K [61] in Figs. 5, 6, and 7, respectively. We can observe the selected images cover a wide range

Table 7: SRCC results of the proposed anchor selection scheme and random selection with KonIQ-10k [7] dataset.

Method	LIVE [53]	CSIQ [24]	KADID-10k [26]	BID [25]	CLIVE [54]	KonIQ-10k [7]
Random Selection	0.954	0.939	0.944	0.881	0.890	0.915
Compare2Score	0.972	0.950	0.952	0.919	0.914	0.931

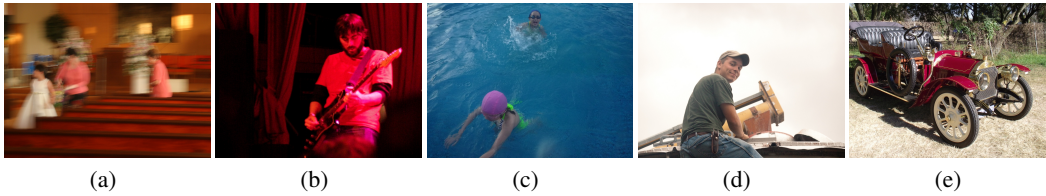


Figure 5: Illustration of the five anchor images selected from KonIQ-10k [7]. (a) MOS = 1.09, $\sigma = 0.29$; (b) MOS = 2.02, $\sigma = 0.39$; (c) MOS = 2.96, $\sigma = 0.38$; (d) MOS = 3.21, $\sigma = 0.41$; (e) MOS = 4.01, $\sigma = 0.34$.

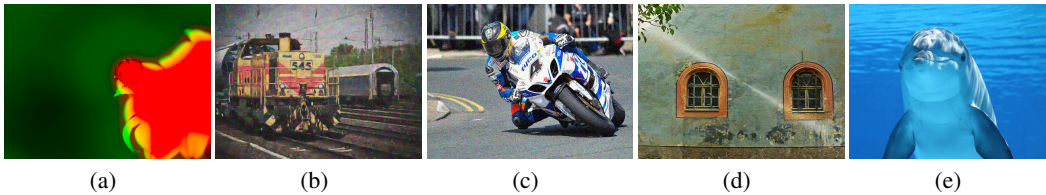


Figure 6: Illustration of the five anchor images selected from KADID-10k [26]. (a) MOS = 1.00, $\sigma = 0.00$; (b) MOS = 1.80, $\sigma = 0.40$; (c) MOS = 2.84, $\sigma = 0.51$; (d) MOS = 3.97, $\sigma = 0.41$; (e) MOS = 4.90, $\sigma = 0.30$.



Figure 7: Illustration of the five anchor images selected from AGIQA-3K [61]. (a) MOS = 0.73, $\sigma = 0.10$; (b) MOS = 0.95, $\sigma = 0.12$; (c) MOS = 2.27, $\sigma = 0.14$; (d) MOS = 3.41, $\sigma = 0.16$; (e) MOS = 3.96, $\sigma = 0.17$.

of visual quality, and the contents of the images are diverse. This robustness of the selection of anchor images effectively supports the model's ability to generalize across different types of visual distortions, enhancing its applicability in real-world IQA scenarios.